

October 2008

Imaging contrast under aperture tip-nanoantenna array interaction

Ji-Young Kim
Purdue University

V.P. Drachev
Birck Nanotechnology Center, School of Electrical and Computer Engineering, Purdue University, vdrachev@purdue.edu

Hsiao-Kuan Yuan
Purdue University - Main Campus, hyuan@purdue.edu

Reuben Bakker
Purdue University - Main Campus, rbakker@purdue.edu

V.M. Shalaev
Birck Nanotechnology Center and School of Electrical and Computer Engineering, Purdue University, shalaev@purdue.edu

Follow this and additional works at: <http://docs.lib.purdue.edu/nanopub>

Kim, Ji-Young; Drachev, V. P.; Yuan, Hsiao-Kuan; Bakker, Reuben; and Shalaev, V. M., "Imaging contrast under aperture tip-nanoantenna array interaction" (2008). *Birck and NCN Publications*. Paper 116.
<http://docs.lib.purdue.edu/nanopub/116>

This document has been made available through Purdue e-Pubs, a service of the Purdue University Libraries. Please contact epubs@purdue.edu for additional information.

Imaging contrast under aperture tip–nanoantenna array interaction

Ji-Young Kim · Vladimir P. Drachev ·
Hsiao-Kuan Yuan · Reuben M. Bakker ·
Vladimir M. Shalaev

Received: 20 June 2008 / Published online: 28 August 2008
© Springer-Verlag 2008

Abstract Periodic arrays of paired and single gold nanorods were imaged in the near field using reflection and transmission modes of a near-field scanning optical microscope at various wavelengths and polarizations of light in the visible range. The paired nanorods act like nanoantenna, and an array of them was initially designed as a negative-index material for the near infrared. Reverse contrast in reflection and transmission images is observed under illumination from the small aperture of a metal-coated fiber probe. By changing the relative orientation of the rods to the polarization, the reverse contrast switches to the normal contrast of near-field imaging. Coupling between the aperture and the nanorod array makes the contrast higher. Transmission through the aperture is enhanced if the aperture probe is positioned between the nanorods. The average near-field transmission exhibits an opposite sign of anisotropy relative to the far-field case. Aperture probes with larger diameters always show normal imaging contrast. The results demonstrate that the broad angular spectra of small-aperture sources play a crucial role in near-field interactions with nanorod arrays. The results also show that angular redistributions of these spectra after transmission or reflection from the nanorod array are likely due to excitation of localized and propagating plasmons.

PACS 07.79.Fc · 71.36.+c · 81.07.-b

J.-Y. Kim · V.P. Drachev (✉) · H.-K. Yuan · R.M. Bakker ·
V.M. Shalaev
School of Electrical and Computer Engineering, Birck
Nanotechnology Center, Purdue University, West Lafayette,
IN 47907, USA
e-mail: vdrachev@ecn.purdue.edu
Fax: +1-765-4962018

1 Introduction

Far-field optics is restricted in the spatial spectrum since only the freely propagating wavevector components with a transverse projection $k_{\parallel} < k$ can be involved. In order to extend the spectrum of spatial frequencies, evanescent waves with $k_{\parallel} \geq k$ should be included. To achieve high resolution with a strongly confined light field, one needs to bring the source (aperture) very close to the sample surface to incorporate evanescent fields. At such small distances, interactions between the sample and source are unavoidable and exhibit unique features depending upon the particulars of the source and sample. It is no surprise that these concepts of near-field optics [1, 2] are tied to the idea of perfect imaging with a metamaterial slab [3]. Improved imaging resolution can be due to either enhanced evanescent fields in a thin metal slab [3] or filtering of the spatial harmonics [4]. In addition, evanescent waves can be excited at the interface of a plasmonic nanostructure and a dielectric and then transferred to far-field propagating electromagnetic waves. Near- to far-field transfer/conversion is a crucial process for imaging with sub-wavelength resolution [3], extraordinary transmittance [5] and light beaming by concentric gratings from an aperture source [6].

The problem of imaging with source–sample interactions is considered here for a metal-coated aperture tip and a nanoantenna array. The arrays under study and our near-field scanning optical microscopy (NSOM) technique are illustrated in Figs. 1 and 2. Several factors, including the angular spectrum of the source, the angular excitation spectra (resonant and non-resonant) of the surface-localized and propagating modes and the angular transmission/reflection spectra (filtering) make overall system analysis rather complicated. In this work we have studied the possible manifestations

Fig. 1 (a) Electron microscopy image of the paired nanorod array. (b) Elementary cell dimensions: $L1$ and $L2$ are the top and bottom lengths, respectively, while $W1$ and $W2$ identify the widths (sample name: $L1, L2, W1, W2, X$ period \times Y period); (paired nanorod: 703 nm, 812 nm, 120 nm, 213 nm, 666×1852); (single nanorod: 691 nm, 781 nm, 104 nm, 205 nm, 666×1806). Vertical structures of paired (c) and single (d) nanorods

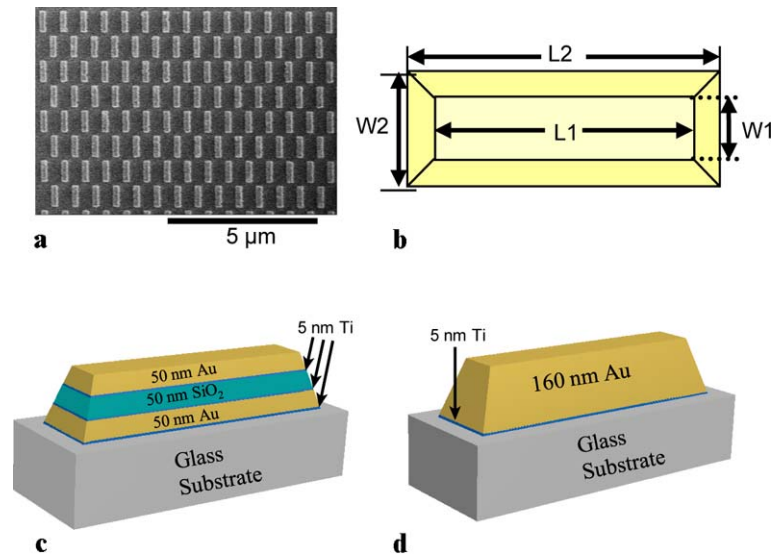
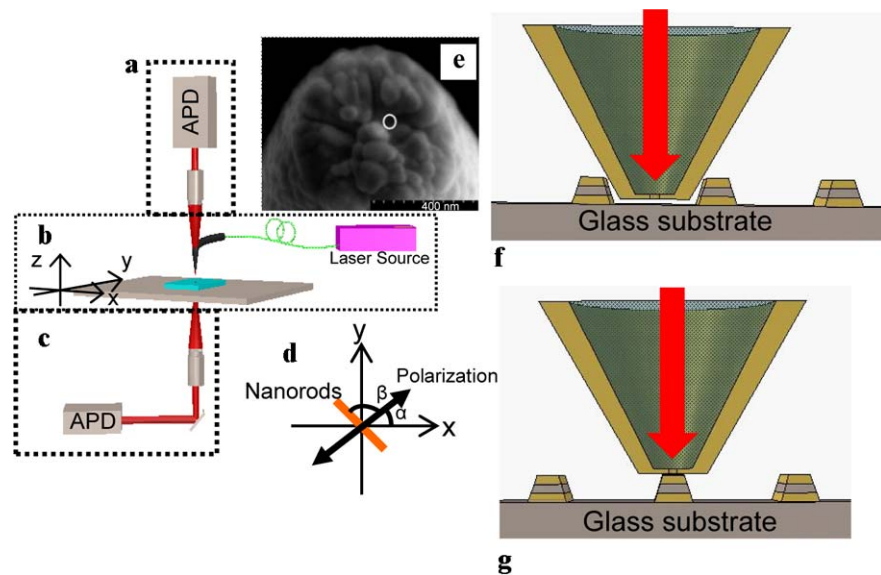


Fig. 2 NSOM: (a) reflection and (c) transmission detection modules; (b) NSOM stage and illumination unit; (d) orientation of the polarization axis and the nanorod; α and β denote the polarization angle and the nanorod orientation angle, respectively; (e) FESEM image of a typical metalized tip where the circle represents the aperture of the tip. Two key relative positions of the tip and paired gold nanorods: a gold-coated tip is in the valley between the nanorods (f) and on top of the nanorod pair (g)



of aperture–sample interactions with respect to imaging in NSOM transmission and reflection modes.

Part of the story concerns the angular dependence of the tip output for both radiative and evanescent fields. The far-field distribution of the angular dependence covers a range wider than $\pm 90^\circ$ and is strongly anisotropic relative to the polarization plane [7]. In the particular case demonstrated in [7], the full width at half maximum (FWHM) of the angular distribution of the far-field intensity was dependent on aperture size. For a 60-nm aperture, the FWHM was about 110° measured in a plane perpendicular to the polarization plane. For the polarization plane, the FWHM was about 150° . This distribution can be approximated by an electric and a magnetic dipole which both lie in the plane of the aperture and are mutually orthogonal [7]. The model given by this pair of dipoles is in good agreement with

experimental far-field measurements for fiber aperture tips coated with metal [7]. The near-field intensity distribution of an aperture probe is also complicated and depends on the geometry of the tip [8]. Phenomena such as local field enhancement at the edges of the metal coating and increases in the effective aperture width due to partial field penetration at the edges of the aperture can frustrate the analysis of near-field results. In addition, if the aperture approaches a dielectric substrate, the transmission power through the probe increases [1]. It has been noted previously that the Fourier transform of the field at the aperture tip exhibits components with the wavevectors of surface plasmon polaritons (SPPs) on metal films [9], even though the SPP wavevectors exceed that of freely propagating light.

The effect of the sample structure on transmission through a single aperture was demonstrated with a concen-

tric grating on both sides of the metal screen [6]. The grating delocalizes the radiation in the near zone of the aperture over the grating. This delocalization leads to either increased transmission or improved directionality of the emitted radiation. Indeed, a small aperture has a strong effect on the divergence of the radiation. A significant portion of the energy stays at the near field of the smooth surface of the screen. However, the grating converts a portion of the near field into propagating fields and allows the energy to reach a distant detector.

Here we discuss the imaging of a subwavelength nanoantenna array using an aperture tip and two of the most common NSOM modes—transmission and reflection scanning modes. A metal-coated fiber tip with a small aperture at the apex serves as the light source. For imaging, the sample is raster scanned under the probe tip, and the transmitted or reflected light is detected in the far field for selected positions. Local variations in the optical properties of a sample appear chiefly as changes in the total detected light. In addition, local optical property variations result in an angular redistribution of the transmitted or reflected intensity pattern. The detected light is collected within a cone given by the angular aperture, i.e. the numerical aperture (NA) of the detection objective. The NA aperture of the 50 \times objective used in this work is 0.45, which corresponds to an angular aperture of $2\theta \approx 53^\circ$. The redistribution of the angular pattern may result in changes in the transmission/reflection images. The transmission pattern can be dependent on the tip position and differs for a hill and a valley [2]. It has also been pointed out that, depending on the detection conditions (allowed or forbidden angles in the total internal reflection condition) [2], a reversed contrast can be detected for small phase objects, while the contrast was the same for amplitude objects. The experiments presented herein show contrast reversal for amplitude objects by varying the aperture probe–sample interaction conditions within the same detection system. Dependence upon both polarization and wavelength is studied. The angular aperture of the collection objective and our planar substrates imply the only allowed light detection.

First we should clarify what are normal and reversed contrasts. For the case of gold nanorods, normal contrast is obvious for the two positions of the tip relative to the topology profile (Fig. 2f and g). At the position above the rod we expect high reflection and low transmission due to possible absorption and scattering at large angles. At the position between the rods, the transmission should be high and the reflection low. This is the case for large-aperture probes with widths in the range of 100–150 nm, which was observed in this work. Such normal behavior is often detected and, in particular, it is observed for paired gold nanorods using a broad-band white-light source [10]. Reversed contrast is opposite to the normal case, with high transmission and low reflection for the position above the nanorod and

low transmission and high reflection for the position between nanorods. Near-field imaging of bean-shaped, double-layer metal structures in transmission mode has shown reversed contrast. The resulting transmission image shows an increased local transmission at the position of each particle in the array [11].

A periodic array of paired gold nanorods as well as an array of single nanorods has been studied here with polarization- and wavelength-controlled near-field microscopy. It has been shown previously that a periodic array of paired gold nanorods manifests an effective negative refractive index at 1.5 μm under far-field illumination at normal incidence [12, 13]. These samples are highly anisotropic. At the parallel polarization along the long axis of the nanorod, both electric and magnetic resonances were obtained in the near-infrared wavelength range for this particular design. Specifically, the symmetric and antisymmetric modes of the paired particles are responsible for the electronic and magnetic properties. All the results of the previous studies, however, are related to plane-wave illumination with the wavevector normal to the substrate surface. The vertically layered structures and their modes under near-field imaging and their possible interaction with a subwavelength aperture light source are less studied. Possible applications of metamaterials imply that near-field interactions with a point-like source (such as a metalized aperture tip, in our case) could provide all possible wavevector directions and polarizations. The study and imaging of anisotropic nanoantenna arrays under the conditions of strong coupling in the combined system is the goal of this work. Near-field interaction with the tip introduces an additional degree of freedom and makes visible light at 532 nm, 633 nm and 785 nm interactive with a combined tip–sample system.

As mentioned above, when the aperture size of the tip is much smaller than the wavelength, the field transmitted through the aperture is strongly localized and enhanced in the vicinity of the aperture, but the transmitted field decreases rapidly away from the aperture [1]. Several manifestations of the near-field interaction between an aperture probe and a sample have been observed. For instance, such interactions cause strong changes in the anisotropy of transmission that are wavelength dependent. Polarization dependence in the reversal contrast is another example. It is due to both anisotropy of the aperture emission pattern and anisotropy of the sample structure. These two sources of anisotropy strengthen each other, providing a contrast value of about 105 in reflection mode for light polarized perpendicular to the long nanorod axis.

The paper is organized as follows. The experimental section presents the sample descriptions and the experimental setup. In the next section, all observed manifestations of the imaging contrast are presented and discussed, including both contrast reversal in reflection with normal contrast in transmission, and contrast reversal in both reflection

and transmission. These experimental results from paired nanorods are compared with those from single nanorod arrays, and we also discuss results from two small-aperture probes. We then consider the anisotropy in the far-field transmission versus the average anisotropy at three wavelengths, obtained from our near-field measurements. Finally, the results are summarized in the conclusion section.

2 Experimental

Both paired and single gold nanorods were prepared on bare glass substrates using electron-beam lithography, photore-sist processing and electron-beam evaporation techniques. First, the geometry of the periodic array was defined in resist by use of an electron-beam writer (JEOL JBX-6000FS) on a glass substrate. Then, a stack of lamellar films was deposited with vacuum electron-beam evaporation. Finally, a lift-off process was performed to obtain the desired gold nanorods.

The stack sequence and thicknesses of the paired nanorod structures are as follows: glass substrate, 5 nm of titanium (Ti), 50 nm of gold (Au), 5 nm of Ti, 50 nm of silicon dioxide (SiO₂), 5 nm of Ti and finally 50 nm of Au. The single nanorod sample comprised a bare glass substrate and a sequence of 5 nm of Ti covered with 160 nm of Au, providing approximately the same height profile and periodicity as the paired nanorod arrays. Two paired nanorod arrays with similar parameters (denoted as sample A and sample B) were used in these studies. Designed to be identical, samples A and B differ primarily in fabrication variations, resulting in a difference of about 5% in elementary cell dimensions. Figure 1a shows a representative, top-down field emission scanning electron microscopy (FESEM) image of the nanorod geometry, while Fig. 1b represents the average measured dimensions of the elementary cell of the nanorod. Realities in the fabrication process due to the e-beam evaporation steps caused the nanorods to have a trapezoidal profile. Lengths L1 and L2 typify the top and the bottom nanorod lengths, respectively, and W1 and W2 represent the top and bottom widths. The sample dimensions were as follows: (sample name: L1, L2, W1, W2, X period × Y period); (sample A: 703 nm, 812 nm, 120 nm, 213 nm, 666 × 1852); (sample B: 670 nm, 780 nm, 112 nm, 220 nm, 642 × 1814); (single nanorod: 691 nm, 781 nm, 104 nm, 205 nm, 666 × 1806). Figure 1c and d illustrate the vertical structure of the paired and single nanorods, respectively.

The far-field transmission and reflection spectra of the samples were measured at normal incidence with a spectroscopy system appropriate for small-area samples. The system contains an ultra-stable tungsten lamp (B&W TEK BPS100), a Glan Taylor prism polarizer, a spectroscopic collection device (SpectraCode/Digilab), a spectrograph (Acton SpectraPro 300i) and a liquid-nitrogen-cooled CCD detector (Roper Scientific). The transmission and reflection

spectra were normalized to a bare substrate and a calibrated silver mirror, respectively. To test that the collection area is less than the sample area, the reflection spectra were first collected from a calibrated aperture in a highly reflective foil (Tedd Pella). The reflected signal was typically less than 1% with this aperture test. Reflection and transmission spectra were collected with incident light at polarizations both parallel and perpendicular to the long axis of the rods.

Near-field studies were carried out using a commercial NSOM (Nanonics MultiView 2000TM) accompanied by a cantilevered aperture probe operating in illumination mode with laser sources at 532 nm, 633 nm and 785 nm. NSOM probes were chosen to have aperture diameters below 100 nm since smaller diameters have been shown to provide better resolution. After several uses, the properties of a tip such as polarization and surface condition were determined, and the tip was then applied for the studies. Specifically, two probes were used for the results presented in this paper. The first was a 50-nm tip pulled from single-mode fiber and coated with Au (150 nm)/Al (50 nm)/Cr (20 nm), and the second was an 80-nm tip pulled from multi-mode fiber with an Au (200 nm)/Cr (20 nm) coating. The results for probes with apertures larger than 150 nm are not shown since they represent normal imaging contrast under all conditions. The experimental NSOM setup is sketched in Fig. 2. The near-field experiments were performed using transmission (Fig. 2b and c) and reflection (Fig. 2a and b) modes with illumination through a fiber aperture probe produced by Nanonics. The FESEM image of the typical metalized tip is shown in Fig. 2 (inset) where the circle represents the aperture of the tip. The transmitted or reflected light was collected by a 50× objective lens with a numerical aperture of 0.45 and measured with an avalanche photodiode (APD). An image is formed by raster scanning the sample and recording the collected light intensity as a function of the scan position. This enables us to obtain topography and NSOM images simultaneously. Two key relative positions of the tip and paired gold nanorods are important for the image contrast; a gold-coated tip is in the valley between the nanorods in Fig. 2f and on top of the nanorod pair in Fig. 2g.

The polarization of light from an NSOM tip is usually induced by the anisotropic geometry (or shape) of the tip and the bending angle and shape of the aperture. Thus, the polarization of light from a particular tip depends on the wavelength, as different wavelengths will interact differently with the tip bend and geometry. In our experimental setup, the polarization of the illuminating light from a fiber tip is measured using a linear polarizer placed after the tip and the objective lens. We define the electric field parallel to the nanorod long axis as the parallel polarization. Figure 2 shows the angular relationships among the polarization axis, the nanorod long axis and the raster scan direction (defined

as the x axis). In Fig. 2d, α is the angle between the polarization axis and the x axis, and β is the angular orientation of the nanorod with respect to the polarization axis. The values of α for each available laser wavelength are: 25° (532 nm), 22° (633 nm) and 138° (785 nm) from the x axis in the counter-clockwise direction. In order to obtain values for β at each wavelength, the nanorod sample was rotated counter-clockwise from the polarization axis, and β was subsequently obtained from NSOM images.

Tips in these experiments were tested by NSOM measurements of a test chromium grating on a glass substrate with a 100-nm height and various periods. In order to confirm the match between the topographical images and the NSOM images, edge areas and defect locations (broken or missing nanorods) of the nanorod samples were scanned, and the resulting topographical and NSOM images were visually compared.

3 Results and discussion

3.1 Far-field optical spectra

The far-field spectra of the nanorod arrays were measured for parallel and perpendicular polarizations over a broad spectral range to compare with the near-field data. Figure 3a and b display the far-field spectra of the paired nanorod sample (sample A) in the perpendicular and parallel polarizations, respectively. Figure 3c and d show the far-field spectra of the single nanorod array with the same polarization

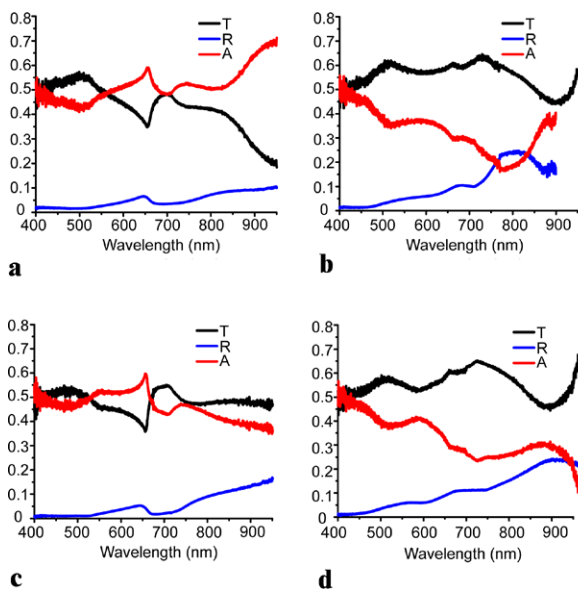


Fig. 3 Far-field spectra of paired nanorod (sample A) ((a) and (b)) and the single nanorod array ((c) and (d)). The *left-hand column* represents the perpendicular polarization while the *right-hand column* is the parallel polarization. *T*: transmission, *R*: reflection and *A*: absorption

arrangement and are similar to the paired nanorods except for the resonance at 950 nm, which is the electrical resonance point of the paired nanorod array.

The sharp minimum at $\lambda = p$ (period) and the broad maximum at longer wavelengths in the far-field transmission spectra are due to Wood's anomalies in the bi-dimensional array [14]. There are two forms of this effect which can occur separately or superimposed. One appears in diffraction gratings at Rayleigh wavelengths if a diffracted order becomes tangent to the plane of the grating. The diffracted beam intensity increases just before the diffracted order vanishes. The second effect comes from a coupling between inhomogeneous diffraction orders and the eigenmodes of the grating. Such a resonance effect can be caused, in particular, by the excitation of the surface plasmon polariton resonance and are called plasmon anomalies. Both the resonant and non-resonant effects are due to the interaction of the diffraction order with the surface. Note that one may try to extend Wood's anomalies onto the near-field aperture source. In our opinion this option does not make much sense and might be confusing. Indeed, the diffraction orders are due to constructive interference of many diffraction units with the same amplitude and phase shift relative to each other under the plane-wave illumination. The notion of diffraction orders loses its sense under illumination with a local source of the size less than a period of the array. While the localized and propagating plasmon resonances can be excited by the sub-wavelength aperture, they do not lead to Wood's anomalies like in the plane wave illumination case.

The far-field spectra show that the absorption is lower and transmission is higher for the parallel polarization; this is in agreement with the finding that the imaginary part of the dielectric function is lower for the parallel polarization due to the size-dependent chemical interface effect and the crystal grains [15].

3.2 Reverse contrast in reflection, enhanced transmission and its polarization dependences

The effects of polarization on the near-field optical properties of a paired nanorod sample (sample A) were studied at 532 nm using the reflection mode of the NSOM system with a 50-nm aperture tip. Figure 4 shows representative topography, reflection and transmission NSOM images for both the perpendicular and parallel polarizations. The arrows indicate the polarization axis for 532 nm. At the quasi-parallel polarization in Fig. 4b, reflected light from the nanorods forms a high-contrast NSOM image that shows even a small cut at the nanorod edge (inside the circle on the figure). The quasi-perpendicular polarization, however, led to reversed contrast in the image, indicated by lower reflection from the nanorod than from the glass substrate area between nanorods, as shown in Fig. 4b, bottom. Surprisingly,

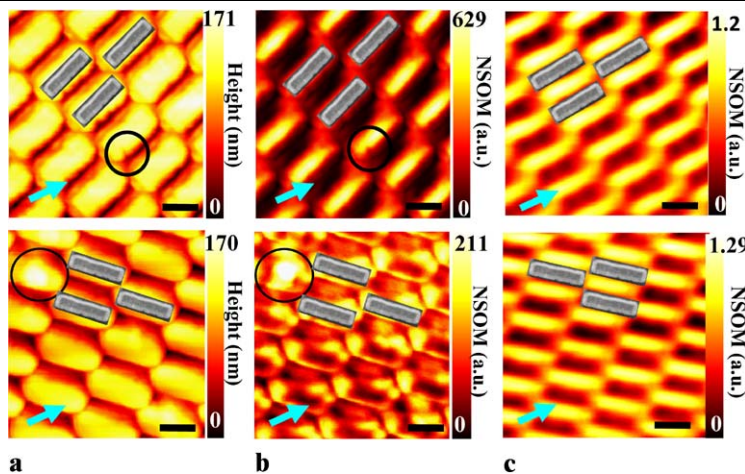
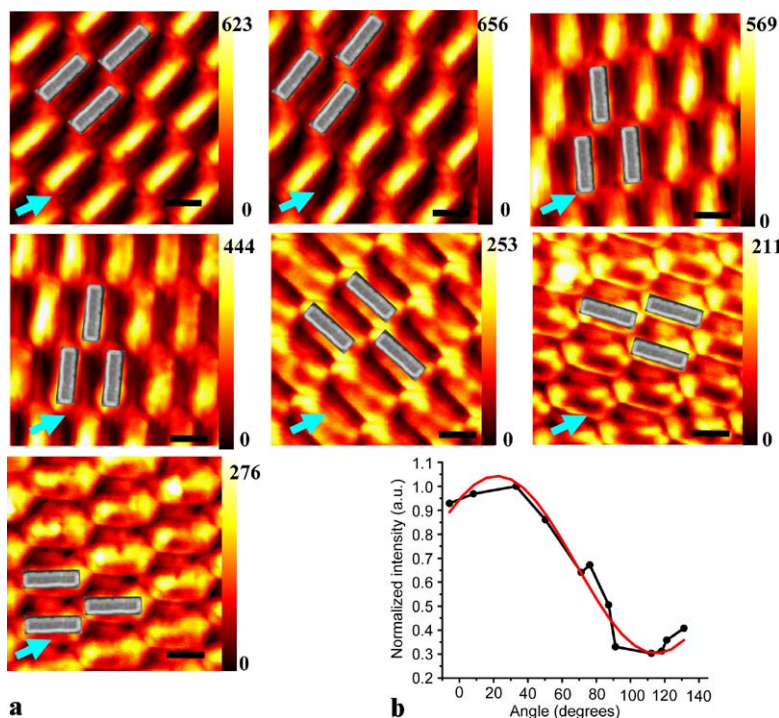


Fig. 4 Reflection and transmission images of a paired gold nanorod array (sample A) at 532 nm: (a) topography images collected with the reflection images. (b) NSOM reflection images (*upper*: quasi-parallel polarization, *lower*: quasi-perpendicular polarization). (c) NSOM transmission images normalized by the light intensity from the aperture

probe measured through the glass. The indented nanorod edge and the gold particle on the nanorod inside the *circles* verify no shift between the topography and NSOM images. *Arrows* represent the polarization axis. *Scale bar* is 500 nm. Representative FESEM images of the nanorods are inserted for the position reference

Fig. 5 (a) Reflection NSOM images at 532 nm. The paired nanorod sample (sample A) was rotated in the counter-clockwise direction from the polarization axis through about 150°. Angle β is 16°, 30°, 72°, 93°, 113°, 140° and 153° from the *left* to *right* and from the *top* to *bottom*. *Arrows* in the NSOM images represent the polarization axis. Representative FESEM images of the nanorods are inserted for the position reference. *Scale bar* is 500 nm. (b) Intensity as a function of sample orientation averaged from 5 $\mu\text{m} \times 5 \mu\text{m}$ reflection NSOM images at 532 nm. NSOM images were normalized by the maximum light intensity at 30°. *Red line* represents a fitted cosine squared function

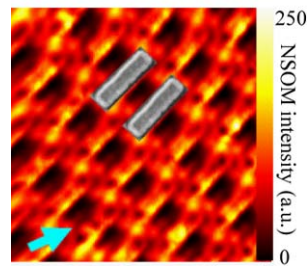


the transmission images (Fig. 4c) demonstrate normal contrast for both polarizations. The switch from normal to reverse contrast in the reflection pattern is detected in detail by gradually changing the relative orientation of the sample and the light polarization. Figure 5 shows the comprehensive polarization dependence of the reflection images at values of the angle β of about 16°, 30°, 72°, 93°, 113°, 140° and 153°. Starting from the parallel polarization, in which the nanorod long axis is parallel to the polarization axis, the

nanorod sample was rotated in the counter-clockwise direction through approximately 150°. As the orientation angle β increased, the initial reflection from the nanorod locations for the parallel polarization dimmed and eventually changed to a situation with a lower reflection from the nanorod than from the glass valley areas between the nanorods.

In order to study the average polarization effect in the nanorod array, the intensity of the collected light was averaged for several 5 $\mu\text{m} \times 5 \mu\text{m}$ NSOM images, encom-

Fig. 6 NSOM reflection image in parallel polarization of the single layered gold nanorod at 532 nm. Scale bar represents 500 nm



passing multiple unit cells. The average intensities are plotted in Fig. 5b, which was obtained from reflection NSOM images at 532 nm. The graph is fitted well with a cosine squared function. A possible origin for the polarization dependence is the scattering in the gap between the nanorods in the perpendicular polarization due to the two side walls of the nanorods. From the obtained intensity patterns of NSOM reflection for both polarizations, the intensity of the valley (the glass between the nanorods) in the perpendicular case is about twice as large as that in the parallel case.

Another interesting observation in these reflection NSOM images is the high contrast of the nanorod in the parallel polarization (16° in Fig. 5a). There is not such a high contrast for the single nanorod arrays of Fig. 6, although both images were obtained under the same experimental conditions.

Near-field transmission imaging is a result of both the angular pattern of the aperture field source and the sample transmission for different components of the angular spectrum. It is no surprise that the average over the image transmission is different from far-field measurements. The anisotropy in the transmission signal is one of the manifestations of this difference. From the far-field spectra, the absorption is lower and the transmission is higher for the parallel polarization. As is mentioned above, this is in agreement with the finding that the imaginary part of the dielectric function is lower for the parallel polarization due to the size-dependent chemical interface effect [15]. The near-field average transmission, however, is different than what is observed from the far-field spectra and causes a change of anisotropy in transmission, which is stressed in Table 1. Here, we define the anisotropy in the transmission as a ratio $(T_{\text{para}} - T_{\text{perp}})/(T_{\text{para}} + T_{\text{perp}})$, which represents the average intensity change of transmission according to the polarization. In Table 1, we see that anisotropy in transmission changes not only in value but also in sign between the near-field and the far-field data. One of the possible reasons for changes in anisotropy is the angular dependence of the tip output for both radiative and evanescent fields. The far-field distribution covers a range wider than $\pm 90^\circ$ and is strongly anisotropic relative to the polarization plane [7].

Table 1 Transmission ratio $((T_{\text{para}} - T_{\text{perp}})/(T_{\text{para}} + T_{\text{perp}}))$ between two polarizations of the near field and the far field. (T_{para} = transmission in parallel polarization, T_{perp} = transmission in perpendicular polarization, NF = near field and FF = far field)

532 nm		633 nm		785 nm	
NF	FF	NF	FF	NF	FF
-0.23	0.07	-0.12	0.2	-0.01	0.08

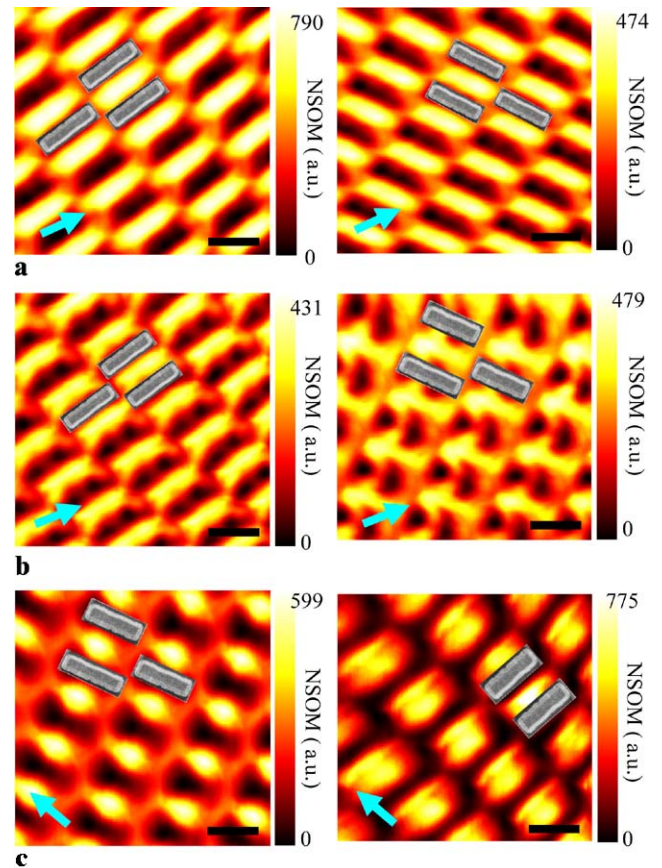


Fig. 7 NSOM transmission images for the single nanorod array sample: (a) 532 nm; (b) 633 nm; (c) 785 nm. The left-hand column is the quasi-parallel polarization, and the right-hand column represents the quasi-perpendicular polarization. Arrows represent the polarization axis. Scale bar is 1 μm

3.3 NSOM transmission imaging in paired and single gold nanorod arrays

Single gold nanorods were also studied for comparison to the paired arrays. The height of the single nanorods was chosen so that the topography would be similar to the paired array case. Under the same experimental conditions as those used for the paired nanorod samples above, single nanorod arrays presented different transmission patterns at incident wavelengths of 532 nm, 633 nm and 785 nm for the perpendicular polarization. Figure 7 shows NSOM transmission images for both the parallel and perpendicular polarizations.

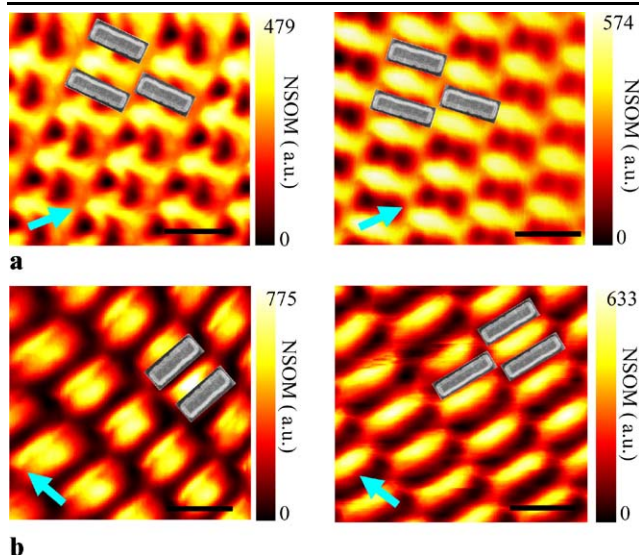


Fig. 8 NSOM transmission images: (a) 633 nm; (b) 785 nm. The *left-hand column* displays the data for the single nanorod array, and the *right-hand column* shows paired nanorod sample (sample A) data. All images are for the quasi-perpendicular polarization. *Arrows* represent the polarization axis. *Scale bar* is 1 μm

At 532 nm (Fig. 7a), essentially normal imaging contrast in transmission is observed for both polarizations, which means that the locations between the nanorods transmit much more light than the positions above the nanorods. At 633 nm (Fig. 7b), however, the transmission pattern is more complicated—a high signal near the center of the nanorod is observed, and the two polarizations show disparate transmission patterns. At 785 nm (Fig. 7c), we again observed reversed transmission patterns through the nanorods. The anomalous transmission patterns at 633 nm and 785 nm were only detectable in the perpendicular polarization.

The near-field interaction of the single nanorod array was different from that of the paired nanorod sample. Figure 8 shows a comparison between the nanorod array types in the perpendicular polarization. As seen in Fig. 8, the paired nanorod array (right-hand column) exhibited essentially normal transmission at both 633 nm and 785 nm, while the single nanorod array (left-hand column) showed some anomalous transmission images at both wavelengths.

3.4 Tip dependence and reversed contrast for both reflection and transmission images

It was mentioned above that since the field distribution out of the aperture tip is sensitive to the diameter, the coating surface and the taper, each tip has different field characteristics. Such a tip dependence is demonstrated by the imaging of the paired nanorod sample using another probe with an aperture size of about 80 nm. We observed reversed contrast images for both reflection and transmission from the

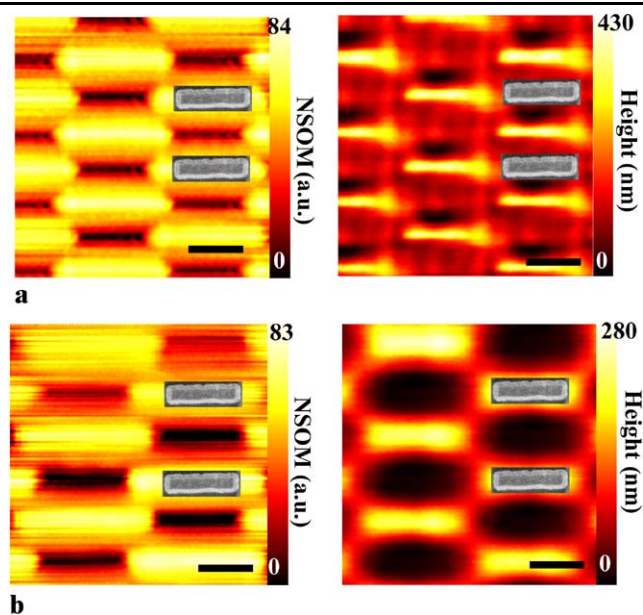


Fig. 9 Scanning results of paired rod array (sample B) using an 80-nm tip at 633 nm with (a) reflection and (b) transmission modes. The *left-hand column* represents topography and the *right-hand column* the NSOM image. The reflection NSOM image shows lower reflection from the nanorod than from the glass, and the transmission NSOM image displays higher transmission through the nanorod than through the glass. *Scale bar* is 500 nm. Each image contains two inserts from a FESEM image

nanorods, which show lower reflection and higher transmission from the nanorods than from the adjacent bare glass between nanorods, as seen in Fig. 9. In the near field, the plasmonic resonance for the paired gold nanorods with such an intricate structure and geometry is complex and includes interactions between the metallic tip and the metal sample. To investigate this effect more precisely, the wavelength was changed to 532 nm, and we again observed lower reflection from the nanorods than from the glass in the NSOM reflection images, as shown in Fig. 10a at 532 nm and Fig. 10b at 633 nm. Figures 9 and 10, on the one hand, were taken using different scanning directions to test the effect scan direction may have on our results, with Fig. 9 scanned left-to-right and Fig. 10 scanned top-to-bottom. Similar results were achieved for each scan direction (compare Fig. 9a right and Fig. 10c, both captured at 633 nm in reflection mode), indicating that the tip used was substantially symmetric and that the results on anomalous transmission and reflection are not artifacts arising from the scan direction.

As we discussed above, in taking NSOM and topography images simultaneously, there exists the possibility of a shift between the two images, which could especially affect the interpretation of images from periodic structures such as our nanorod arrays. In order to confirm that no shift existed between our topography and NSOM images, we used defects such as identifiable broken nanorods for reference location indicators. As an example, Fig. 11a shows the topog-

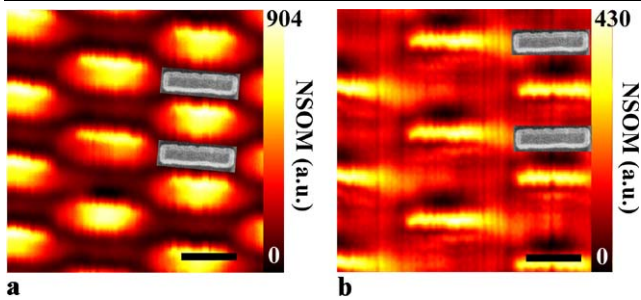


Fig. 10 NSOM images in reflection mode for paired nanorod array (sample B) with 80-nm probe: (a) 532 nm, (b) 633 nm. At 532 nm, higher contrast is observed. The scanning direction is top-to-bottom as compared with Fig. 9, which has a left-to-right scanning direction. Scale bar is 500 nm

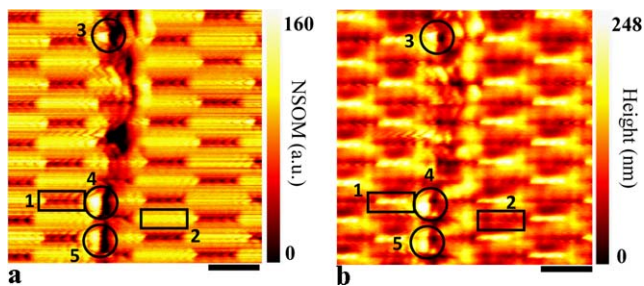


Fig. 11 Reflection images at 633 nm: (a) Topography and (b) NSOM image. Circles 3, 4, and 5 represent broken nanorods. Broken gold particles reflect more light than the empty areas or the glass substrate. Rectangle 1 is the gap between nanorods, which shows higher reflection in the NSOM image. Rectangle 2 is the intact nanorod, which shows lower reflection similar to the case for Fig. 9. These images confirm the lack of a shift between the NSOM and topography images while also supporting the results of Fig. 9. Scale bar is 1 μm

raphy and Fig. 11b the reflection NSOM image of a line of defective nanorods, which provided a very useful location reference. In the NSOM image of Fig. 11b, the malformed nanorods reflected more light than glass while the empty parts of the malformed nanorods showed low reflection, as indicated by circles 3, 4 and 5. This is consistent with the topography image of Fig. 11a and confirms that there is no shift between the images. However, the gap (glass substrate) between intact nanorods indicated by rectangle 1 of Fig. 11a displayed higher reflection than nanorods in the NSOM image of Fig. 11b, and also the intact nanorod in rectangle 2 presented lower reflection than the glass substrate in the NSOM image, confirming our anomalous results from Fig. 9.

4 Conclusions

In conclusion, we have studied the near-field interactions of paired gold nanorod arrays with an NSOM aperture tip, which introduces an additional degree of freedom and makes possible the excitation of plasmon modes in the combined

system of the tip and the metal nanostructure in the visible range. The metalized aperture tip supports both outgoing propagating and evanescent waves. The angular distribution of these waves is very broad for small apertures and anisotropic in two orthogonal planes, both containing the fiber tip axis. The nanostructure array can transfer an evanescent wave into the far field due to coupling between the tip output and the nanostructure array, and out-coupling can occur due to SPP reradiation as propagating light or due to scattering changes in the transmission or reflection. The specific features of transmission and reflection under near-field excitation found in this work indicate a strong redistribution in the angular pattern of the aperture source. Indeed, the radiation, going at the large angles, does not match an angular aperture of the detection system. The 30% percent enhanced transmission through the aperture probe placed between the nanorods indicates that a portion of the large-angle radiation is redirected to the small, detected angles.

Two basic manifestations of the near-field interaction were demonstrated. First, strong changes in the anisotropy of transmission were observed indicating strong contribution from the large angle propagating and evanescent waves in the polarization dependence of transmission through the nanorod array. Secondly, the reversed contrast of near-field imaging in transmission and reflection is both polarization and wavelength dependent. These observations are structurally sensitive, as follows from the comparison data for paired and single nanorod arrays of the same height profile. The contrast with large (>100 nm) aperture probes is always normal. Specific properties of the small-aperture probes affect the imaging contrast in its deviation from the normal.

Acknowledgements The authors are grateful to W. Cai and S. Xiao for their assistance with the measurement of the far-field spectra and Mark Thoreson and Josh Borneman for their help in manuscript preparation. This work was supported in part by ARO-MURI Award 50342-PH-MUR and NSF-PREM Grant DMR-0611430.

References

1. L. Novotny, B. Hecht, *Principles of Nano-optics* (Cambridge University Press, New York, 2006)
2. B. Hecht, H. Bielefeldt, D.W. Pohl, L. Novotny, H. Heinzelmann, *J. Appl. Phys.* **84**, 5873 (1998)
3. J.B. Pendry, *Phys. Rev. Lett.* **85**, 3966 (2000)
4. G. Fedorov, S.I. Maslovski, A.V. Dorofeenko, A.P. Vinogradov, I.A. Ryzhikov, S.A. Tretyakov, *Phys. Rev. B* **73**, 035409 (2006)
5. T.W. Ebbesen, H.J. Lezec, H.F. Ghaemi, T. Thio, P.A. Wolf, *Nature* **391**, 667 (1998)
6. H.J. Lezec, A. Degiron, E. Devaux, T.W. Ebbesen, *Science* **297**, 820 (2002)
7. C. Obermüller, K. Karrai, *Appl. Phys. Lett.* **67**, 3408 (1995)
8. B. Hecht, B. Sick, V. Dectert, R. Zenobi, O.J.F. Martin, D.W. Pohl, *J. Chem. Phys.* **112**, 7761 (2000)

9. B. Hecht, H. Bielefeldt, L. Novotny, Y. Inouye, D.W. Pohl, *Phys. Rev. Lett.* **77**, 1889 (1996)
10. R.M. Bakker, V.P. Drachev, H.-K. Yuan, V.M. Shalaev, *Physica B* **394**, 137 (2007)
11. R.M. Bakker, V.P. Drachev, H.-K. Yuan, V.M. Shalaev, *Opt. Express* **12**, 3701 (2004)
12. V.M. Shalaev, W. Cai, U.K. Chettiar, H.K. Yuan, A.K. Sarychev, V.P. Drachev, *Opt. Lett.* **30**, 3356 (2005)
13. V.P. Drachev, W. Cai, U.K. Chettiar, H.K. Yuan, A.K. Sarychev, A.V. Kildishev, G. Klimeck, V.M. Shalaev, *Laser Phys. Lett.* **3**, 49 (2006)
14. M. Sarrazin, J.-P. Vigneron, J.-M. Vigoureux, *Phys. Rev. B* **67**, 085415 (2003)
15. V.P. Drachev, U. Chettiar, A.V. Kildishev, H.K. Yuan, W. Cai, V.M. Shalaev, *Opt. Express* **16**, 1186 (2008)